

Experimental study of the $e^+e^- \rightarrow \pi^0\gamma$ process in the energy region $\sqrt{s} = 0.60 - 0.97$ GeV.

M.N.Achasov, K.I.Beloborodov, A.V.Berdugin,
A.G.Bogdanchikov, A.V.Bozhenok, A.D.Bukin, D.A.Bukin,
T.V.Dimova, V.P.Druzhinin, V.B.Golubev, V.N.Ivanchenko,
A.A.Korol, S.V.Koshuba, E.V.Pakhtusova, A.A.Polunin,
E.E.Pyata, A.A.Salnikov, S.I.Serednyakov, V.V.Shary,
Yu.M.Shatunov, V.A.Sidorov, Z.K.Silagadze, A.N.Skrinsky,
A.G.Skripkin, Yu.V.Usov, A.A.Valishev, A.V.Vasiljev

November 5, 2018

Abstract

Results of the study of the $e^+e^- \rightarrow \pi^0\gamma$ process with SND detector at VEPP-2M collider in the c.m.s. energy range $\sqrt{s} = 0.60 - 0.97$ GeV are presented. Using 36513 selected events corresponding to a total integrated luminosity of 3.4 pb^{-1} the $e^+e^- \rightarrow \pi^0\gamma$ cross section was measured. The energy dependence of the cross section was analyzed in the framework of the vector meson dominance model. The data are well described by a sum of $\phi, \omega, \rho \rightarrow \pi^0\gamma$ decay contributions with measured decay probabilities: $Br(\omega \rightarrow \pi^0\gamma) = (9.34 \pm 0.15 \pm 0.31)\%$ and $Br(\rho^0 \rightarrow \pi^0\gamma) = (5.15 \pm 1.16 \pm 0.73) \times 10^{-4}$. The $\rho - \omega$ relative interference phase is $\varphi_{\rho\omega} = -10.2 \pm 6.5 \pm 2.5^\circ$.

1 Introduction

Cross section of the $e^+e^- \rightarrow \pi^0\gamma$ process at the c.m.s. energies $\sqrt{s} = 0.60 - 0.97$ GeV within the framework of the vector meson dominance model is determined by radiative decays of light vector mesons $\rho^0(770)$, $\omega(782)$, $\phi(1020)$. These decays belong to the class of magnetic dipole transitions and represent major interest for study of quark structure of vector mesons and for tests of low-energy models of strong interactions, such as non-relativistic quark model, effective potential models, etc. [1, 2, 3, 4, 5]. Study of this process allows to improve accuracy of the parameters of the $\rho^0, \omega \rightarrow \pi^0\gamma$ decays.

The only previous measurement of the decay $\rho^0 \rightarrow \pi^0\gamma$ was carried out by ND detector [6]: $Br(\rho^0 \rightarrow \pi^0\gamma) = (7.9 \pm 2.0) \times 10^{-4}$. This result agrees with the PDG value for isotopically complementary channel: $Br(\rho^\pm \rightarrow \pi^\pm\gamma) = (4.5 \pm 0.5) \times 10^{-4}$ [10]. The $\omega \rightarrow \pi^0\gamma$ decay was studied in several experiments

[6, 11, 12, 13, 14, 15]. The world average decay probability $Br(\omega \rightarrow \pi^0\gamma) = (8.7 \pm 0.4)\%$ [10].

In this work we present the study of the $e^+e^- \rightarrow \pi^0\gamma$ process with SND detector at VEPP-2M collider.

2 Detector and experiment

The SND detector [16] consists of an electromagnetic calorimeter, tracking and muon systems. The main part of the detector is a three-layer spherical electromagnetic calorimeter consisting of 1600 NaI(Tl) crystals. Total thickness of the calorimeter for the particles flying from the interaction point is $13.4 X_0$. Total solid angle is $90\% \cdot 4\pi$. The energy resolution of the calorimeter for photons is $\sigma_E/E \approx 4.2\%/E(\text{GeV})^{1/4}$, the angular resolution is $\sigma_{\varphi,\theta} \approx 0.82^\circ/\sqrt{E(\text{GeV})} \oplus 0.63^\circ$.

The experiment was carried out at VEPP-2M collider [17] with SND detector [16]. The data were collected in March – July, 1998 [18] at 30 points in the energy range $\sqrt{s} = 0.60 - 0.97$ GeV. The total integrated luminosity used for the analysis was $\sim 3.4 \text{ pb}^{-1}$. The beam energy determination was based on measured magnetic field in the bending magnets and beam revolution frequency in the collider. The error of the center of mass energy determination consists of two parts: 0.1 MeV — relative accuracy of energy setting for each energy point and 0.2 MeV — general energy scale bias common for all points within the experiment.

3 Data analysis

In this work the process $e^+e^- \rightarrow \pi^0\gamma$ was studied in the three-photon final state. The main sources of background are QED processes $e^+e^- \rightarrow 3\gamma$ and $e^+e^- \rightarrow 2\gamma$ with extra photons of the machine background. Other possible sources are process $e^+e^- \rightarrow \eta\gamma$, and cosmic background.

3.1 Events selection

For an event to be recorded the SND first level trigger (FLT) required at least two clusters of hit crystals in the calorimeter and no signals in neither tracking nor muon systems. The FLT threshold on calorimeter energy deposition changed with the beam energy, but was always below $0.4\sqrt{s}$.

The reconstructed events were first put through primary selection which required at least 3 neutral and no charged particles, total energy deposition $E_{tot} > 0.65\sqrt{s}$, total momentum measured by the calorimeter $P_{tot} < 0.3\sqrt{s}$, polar angles of the two highest energy photons $36^\circ < \theta_{1,2} < 144^\circ$, the polar angle of the third photon (descending order in energy) $27^\circ < \theta_3 < 153^\circ$, and the energy deposition of this photon $E_{p3} > 0.1\sqrt{s}$. These conditions select three-photon events, suppress machine background and two photon annihilation

events with additional background clusters in the calorimeter. As a result 52415 events were selected for further analysis.

In order to improve energy and angular resolution for photons the selected events were kinematically fitted with total energy and momentum conservation constraints. The fit results are the value of $\chi^2_{3\gamma}$ of the hypothesis and fitted kinematical parameters of the photons. The kinematic fit improves resolution in invariant mass of photon pairs from π^0 decays from 11.2 MeV to 8.6 MeV (Fig.1).

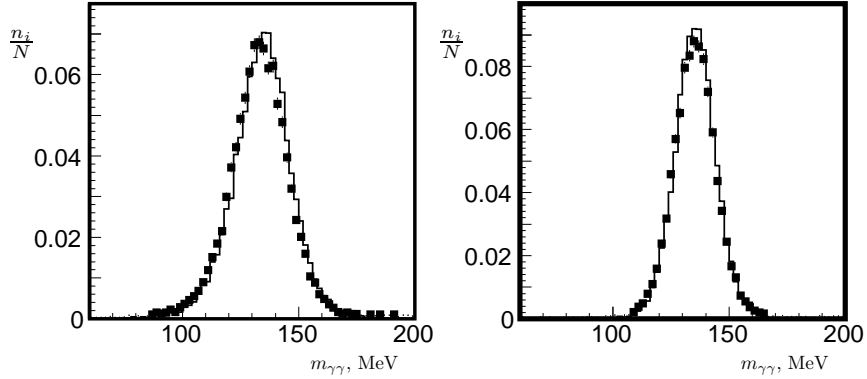


Figure 1: Invariant mass distribution for photons pairs in $e^+e^- \rightarrow \pi^0\gamma$ events before (left) and after (right) kinematic fitting. Solid line — MC simulation, points — data ($\sqrt{s} = 782$ MeV).

The $\chi^2_{3\gamma}$ distribution is shown in Fig.2. For additional suppression of cosmic and machine backgrounds we required $\chi^2_{3\gamma} < 20$. This cut also implicitly limits maximum energy of initial state radiation (ISR) photons in the process under study (Fig.3). In order to suppress 2-photon annihilation background, each selected event was kinematically fitted to $e^+e^- \rightarrow 2\gamma$ hypothesis and restriction on calculated $\chi^2_{2\gamma}$ was applied: $\chi^2_{3\gamma} - \chi^2_{2\gamma} < 0$. The $\chi^2_{3\gamma} - \chi^2_{2\gamma}$ distribution is shown in Fig.2.

The only significant backgrounds to the process under study remaining after described above cuts are $e^+e^- \rightarrow \eta\gamma$ and QED 3γ annihilation. In the latter process all kinematically allowed combinations of the photon energies and angles are present, so this background cannot be completely eliminated and must be subtracted. To this end all events, which passed primary selection and kinematic fit cuts, were divided into two classes: events with $108 \text{ MeV} \leq m_{\gamma\gamma} \leq 162 \text{ MeV}$ were assigned to class **A**, the rest — to class **B**. Here $m_{\gamma\gamma}$ is an invariant mass of a photon pair after kinematic fitting (Fig.1). The total number of the selected class **A** events is 36513. The fraction of $e^+e^- \rightarrow \eta\gamma$ background in this class is less than 0.1%. For the class **B** this fraction is up to 5%. For calculation of integrated luminosity the special sample of $e^+e^- \rightarrow 2\gamma$ events (class **C**) was selected using following criteria: no charged particles, at least two neutral particles, energy depositions for two most energetic photons $E_{p1,2} > 0.3\sqrt{s}$,

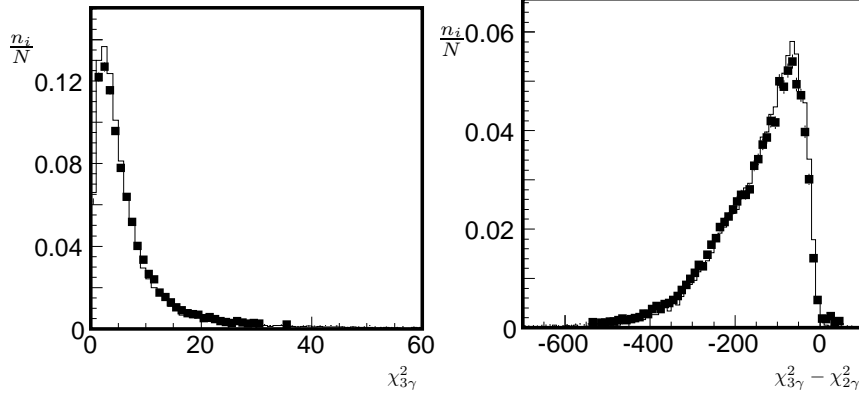


Figure 2: Distributions over $\chi^2_{3\gamma}$ (left) and $\chi^2_{3\gamma} - \chi^2_{2\gamma}$ (right) for class **A** selection. Solid line — MC simulation, points — experiment ($\sqrt{s} = 782$ MeV).

their polar angles $36^\circ < \theta_{1,2} < 144^\circ$, azimuth acollinearity $\Delta\varphi_{12} < 10^\circ$, polar acollinearity $\Delta\theta_{12} < 25^\circ$, event does not belong to classes **A** or **B**. It is necessary to note significant contribution of $e^+e^- \rightarrow \pi^0\gamma$ events to the class **C** (up to 10% at $\omega(782)$ resonance).

3.2 Cross section parameterization

The $e^+e^- \rightarrow \pi^0\gamma$ cross section in the framework of VDM can be parameterized as follows [26, 28]:

$$\sigma_{\pi^0\gamma}(s) = \frac{(4\pi)^2 \alpha \cdot q(s)^3}{3s^{3/2}} \left| \sum_{V=\rho,\omega,\phi} \frac{g_{\gamma V} \cdot g_{V\pi^0\gamma}}{D_V(s)} + A_{nonres} \right|^2, \quad (1)$$

$$D_V(s) = m_V^2 - s - i\sqrt{s}\Gamma_V(s), \quad (2)$$

$$q(s) = \frac{\sqrt{s}}{2} \left(1 - \frac{m_{\pi^0}^2}{s} \right). \quad (3)$$

Here $g_{\gamma V}$ and $g_{V\pi^0\gamma}$ are coupling constants, m_V is the V resonance mass, $\Gamma_V(s)$ is the energy-dependent width of the resonance taking into account processes with branching ratios larger than 1%, A_{nonres} represents possible non-resonant contribution. Using following formulas for coupling constants:

$$|g_{\gamma V}| = \sqrt{\frac{m_V^5}{(4\pi)^2 \alpha} \Gamma_V \sigma_V}, \quad (4)$$

$$|g_{V\pi^0\gamma}| = \sqrt{\frac{3\Gamma_V}{q(m_V^2)^3} \frac{\sigma_{V\pi^0\gamma}}{\sigma_V}}, \quad (5)$$

where σ_V and $\sigma_{V\pi^0\gamma}$ are cross sections of $e^+e^- \rightarrow V$ and $e^+e^- \rightarrow V \rightarrow \pi^0\gamma$ for $\sqrt{s} = m_V$, Eq.(1) can be transformed to the form more suitable for data

approximation:

$$\sigma_{\pi^0\gamma}(s) = \frac{q(s)^3}{s^{3/2}} |A_{\rho^0\pi^0\gamma}(s) + A_{\omega\pi^0\gamma}(s) + A_{\varphi\pi\gamma}(s) + a_{\pi^0\gamma}|^2, \quad (6)$$

$$A_V(s) = \frac{m_V \Gamma_V f_V(s)}{D_V(s)} \sqrt{\frac{m_V^3}{q(m_V^2)^3}} \sigma_{V\pi^0\gamma}, \quad (7)$$

where $a_{\pi^0\gamma}$ is a non-resonant contribution. We used two different models for description of interference phase between $\rho, \omega \rightarrow \pi^0\gamma$ decay amplitudes. For model with energy-independent interference phases, $f_{\rho,\varphi} = e^{i\varphi_{\rho,\varphi}}$, $f_\omega \equiv 1$. In this case the φ_ρ is expected to be 0° for pure ρ and ω isotopic states. Electromagnetic ρ - ω mixing leads to nonzero value of φ_ρ . It can be estimated from $B(\omega \rightarrow 2\pi)$: $\varphi_\rho \approx -13^\circ$. The second model is based on mixed propagator approach [27, 28]:

$$f_{\rho,\omega}(s) = \frac{r_{\rho,\omega}(s)}{|r_{\rho,\omega}(m_V^2)|} \quad , \quad f_\phi(s) = e^{i\varphi_\phi}, \quad (8)$$

$$r_\omega(s) = 1 + \varepsilon(s) \cdot \left(\frac{|g_{\gamma\rho^0}|}{|g_{\gamma\omega}|} + \frac{|g_{\rho^0\pi^0\gamma}|}{|g_{\omega\pi^0\gamma}|} \right), \quad (9)$$

$$r_\rho(s) = 1 - \varepsilon(s) \cdot \left(\frac{|g_{\gamma\omega}|}{|g_{\gamma\rho^0}|} + \frac{|g_{\omega\pi^0\gamma}|}{|g_{\rho^0\pi^0\gamma}|} \right), \quad (10)$$

$$\varepsilon(s) = \frac{\Pi_{\rho\omega}}{D_\omega(s) - D_\rho(s)}, \quad (11)$$

where $\Pi_{\rho\omega}$ is $\rho - \omega$ mixing self-energy.

Detection efficiency for $e^+e^- \rightarrow \pi^0\gamma$ process depends not only on c.m.s. energy \sqrt{s} but also on energy of extra photons emitted by initial particles E_r . The detection efficiency $\varepsilon_r(\sqrt{s}, E_r)$ was determined by Monte Carlo simulation with ISR taken into account. The energy and angular distributions of ISR photons were generated according to Refs. [21, 22]. The dependence of detection efficiency on E_r approximated by a smooth function is shown in Fig.3 for $\sqrt{s} = 782$ MeV. The noticeable peak in detection efficiency near ISR kinematic limit corresponds to the case when $\pi^0\gamma$ invariant mass is close to m_{π^0} and ISR photon is emitted at the large angle and detected. The effective threshold on the ISR photon energy $\delta E_r(s)$ is determined by χ^2 restriction and can be defined as a width at half maximum of the $\varepsilon_r(\sqrt{s}, E_r)$. At $\sqrt{s} = 782$ MeV $\delta E_r \approx 64.4$. The δE_r dependence on \sqrt{s} is shown in Fig.3.

The visible cross section of the $e^+e^- \rightarrow \pi^0\gamma$ process was calculated as [20]:

$$\sigma_{vis}(s) = \int_0^{\frac{2E_{r,max}}{\sqrt{s}}} \varepsilon_r(\sqrt{s}, \frac{x\sqrt{s}}{2}) F(x, s) \sigma((1-x)s) dx \quad (12)$$

where $\sigma(s)$ is cross section, the function $F(x, s)$ is electron “radiator” function [21]. For data presentation we used traditional form:

$$\sigma_{vis}(s) = \varepsilon(\sqrt{s}) \cdot \beta(\sqrt{s}) \cdot \sigma(s)$$

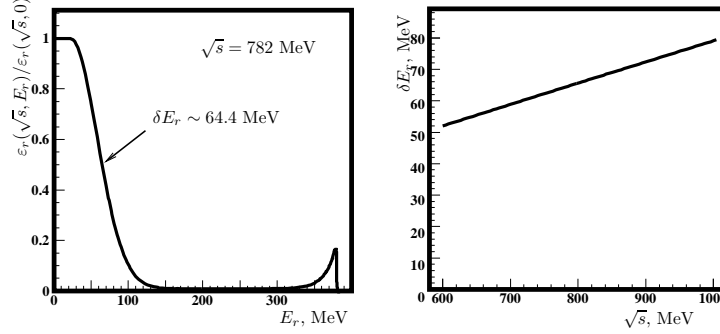


Figure 3: Detection efficiency as function of the extra photons energy $\varepsilon_r(\sqrt{s}, E_r)$ for $\sqrt{s} = 782$ MeV (left) and effective extra photons energy threshold δE_r (right) as function of \sqrt{s} .

where $\varepsilon(\sqrt{s})$ and $\beta(\sqrt{s})$ are defined as:

$$\varepsilon(\sqrt{s}) \equiv \varepsilon_r(\sqrt{s}, 0) \quad (13)$$

$$\beta(\sqrt{s}) \equiv \frac{\int_0^{\frac{2E_{r,max}}{\sqrt{s}}} \varepsilon_r(\sqrt{s}, \frac{x\sqrt{s}}{2}) F(x, s) \sigma((1-x)s) dx}{\varepsilon_r(\sqrt{s}, 0) \cdot \sigma(s)} \quad (14)$$

For simulation of the background process $e^+e^- \rightarrow 3\gamma$ (QED) the lowest-order formulas from [23] were used. Visible cross section calculated using Monte Carlo simulation was corrected for higher order loop diagrams and soft photons emission [24] using δE_r as an upper limit of soft photons energy. The correction varied in the range of 0.915 – 0.925. We expect that the accuracy of the calculated $e^+e^- \rightarrow 3\gamma$ visible cross section is not worse than 2%.

For simulation of the process $e^+e^- \rightarrow 2\gamma$ (QED) used for luminosity determination the formula from [25] taking into account additional photon emission was used. The accuracy of the visible cross section determination is estimated as 1%.

3.3 Data approximation

The FIT package [20] was used for data fitting. The fitting was done by means of maximum likelihood method on all three data sets (classes **A**, **B**, and **C**) simultaneously. Expected number of events in the i -th energy point was calculated as:

$$N_i^{(j)} = IL_i \cdot (\sigma_{\pi^0\gamma,vis}^{(j)}(E_i) + \sigma_{3\gamma,vis}^{(j)}(E_i) + \sigma_{\eta\gamma,vis}^{(j)}(E_i)); j = A, B;$$

$$IL_i = \frac{N_i^{(C)}}{\sigma_{2\gamma,vis}^{(C)}(E_i) + \sigma_{\pi^0\gamma}^{(C)}(E_i)}.$$

Visible hadronic cross sections were calculated according to Eq.(12) and corrected for beam energy spread. Because the $e^+e^- \rightarrow \pi^0\gamma$ process gives notice-

able contribution to events of luminosity process $e^+e^- \rightarrow 2\gamma$, the integrated luminosity (IL_i) was recalculated on every iteration step of the minimization. The accuracy of determination of the c.m.s. energy is worse than the accuracy of the ω -meson mass value. Therefore we introduced the possible energy scale bias ΔE as a free parameter. Other fit parameters were $\sigma_{\omega\pi^0\gamma}$, $\sigma_{\rho\pi^0\gamma}$, $a_{\pi^0\gamma}$, φ_ρ or $\Pi_{\rho\omega}$ depending on approach to phase factor (Eqs.(1)–(8)) calculation, and $k_{3\gamma}$. The $k_{3\gamma}$ parameter is a ratio of measured and calculated $\sigma_{3\gamma}$ cross sections. Parameters of the process $e^+e^- \rightarrow \phi \rightarrow \pi^0\gamma$ were taken from [29]:

$$\sigma_{\phi\pi^0\gamma} = 5.12 \pm 0.39 \text{ nb} \quad (15)$$

$$\varphi_\phi = 158 \pm 11^\circ \quad (16)$$

For other cross section parameters the world average values [10] were used.

Data were approximated in four models:

1. $\sigma_{\rho^0\pi^0\gamma} = 0$, $a_{\pi^0\gamma} = 0$,
2. $\sigma_{\rho^0\pi^0\gamma}$ and φ_{ρ^0} are free parameters, $a_{\pi^0\gamma} = 0$,
3. $\sigma_{\rho^0\pi^0\gamma}$ is a free parameter, $a_{\pi^0\gamma} = 0$, $\Pi_{\rho\omega}$ is a free parameter,
4. $\sigma_{\rho^0\pi^0\gamma}$ is a free parameter, $a_{\pi^0\gamma}$ is a free real parameter, $\Pi_{\rho\omega}$ calculated from $B(\omega \rightarrow 2\pi)$.

Obtained energy scale bias (ΔE) is -0.34 ± 0.08 MeV for all models. It is consistent with our expectations. Found value of $k_{3\gamma}$ is $98.7 \pm 1.3\%$ with $\frac{\chi^2}{N} = \frac{26}{29}$ shows good agreement between calculated and measured cross sections of QED 3γ annihilation. For background subtraction we used the measured cross section. Other obtained parameters are listed in the Table 1.

Table 1: The fitted cross section parameters for different models. Only statistical errors are shown.

	$\sigma_{\omega\pi^0\gamma}$, nb	$\sigma_{\rho^0\pi^0\gamma}$, nb	$\varphi_{\rho\omega}$, $^\circ$	$\Pi_{\rho\omega}$, MeV ²	$Re a_{\pi^0\gamma}$, nb ^{$\frac{1}{2}$}	χ^2/N
1	176.6 \pm 1.4	0			0	81/28
2	155.8 \pm 2.7	0.58 \pm 0.13	-10.2 \pm 6.5		0	21.6/26
4	155.9 \pm 2.7	0.56 \pm 0.13	-9.9 \pm 6.5 ¹⁾	-2819 \pm 1841	0	21.9/26
3	156.8 \pm 2.8	0.51 \pm 0.13	-12.8 \pm 1.1 ¹⁾	-3676 \pm 303 ²⁾	-0.13 \pm 0.13	20.7/25

¹⁾calculated using Eqs.(8)–(11)

²⁾derived from $B(\omega \rightarrow 2\pi)$

Large χ^2 value for the first model shows that $e^+e^- \rightarrow \pi^0\gamma$ cross section cannot be described only by ω and ϕ decays contribution. The second model corresponds to an energy independent $\rho - \omega$ interference phase. Obtained value of this phase $(-10.2 \pm 6.5)^\circ$ is in agreement with expectation from electromagnetic $\rho - \omega$ mixing $\varphi_\rho = (-12.8 \pm 1.1)^\circ$. Therefore the last two fits were performed in mixed propagator approach (Eq.(8)). Mixing self-energy $\Pi_{\rho\omega}$ was

taken as a free parameter for the model 3 and calculated from the world average $B(\omega \rightarrow 2\pi)$ for the model 4. The model 4 was used to estimate the contribution from higher vector resonances ρ' , ω' , which was introduced as a pure real parameter $a_{\pi^0\gamma}$. The fitted value of $a_{\pi^0\gamma}$ is compatible with zero. All the models 2 – 4 describe the experimental data equally well.

3.4 Systematic errors.

Systematic error contributions for obtained cross section parameters are summarized in the Table 2.

Systematic error of luminosity determination originates mostly from inaccuracy in cross section calculation (1%) and uncertainty of detection efficiency of the luminosity process, which was estimated using different angle and acollinearity selection cuts. The total error of the integrated luminosity determination was $\sim 2 - 3\%$.

Primary selection efficiency depends on simple kinematic cuts and is independent of c.m.s. energy. Thus, its systematic error emerging from simulation inaccuracy was studied by comparison of simulated and experimental event distributions at ω -resonance peak, where backgrounds are negligible. Systematic error of primary selection efficiency does not exceed 1.5%.

Table 2: Contributions to the systematic errors of the cross section parameters

Source	$\sigma_{\omega\pi^0\gamma}$	$\sigma_{\rho^0\pi^0\gamma}$	φ
Integrated luminosity	2.0%	3.1%	8%
Three photons selection efficiency	1.5%	1.5%	4%
Final selection efficiency	1.6%	5.6%	22%
Additional clusters	0.3%	1%	2%
PDG table errors	0.1%	4%	4%
Total (no model error)	3.0%	9.0%	24%

The machine background changed with c.m.s. energy. To study its influence on detection efficiency we merged recorded experimental background events with the simulated ones. Comparison of detection efficiencies obtained by simulation with and without merging machine background gives an estimate of the detection efficiency error from this source, not exceeding 0.5%.

The final class **A** selection conditions contain cuts in invariant masses and complex kinematic parameters $\chi_{3\gamma}^2$, $\chi_{2\gamma}^2$. Dependences of their efficiencies on c.m.s. energy and ISR photon energy in experiment and simulation may differ. In order to evaluate systematic error coming from this source, approximations were done with different cuts in these parameters.

Substantial systematic error contributions to the $\sigma_{\rho^0\pi^0\gamma}$ and φ come from inaccuracy of PDG data, mostly from the Γ_ω uncertainty.

Table 3: $e^+e^- \rightarrow \pi^0\gamma$ cross section. δE is a c.m.s. energy spread, IL is an integrated luminosity, N is a number of events, N_{bg} is an estimated number of background events, $\varepsilon_{\pi^0\gamma}$ is detection efficiency (Eq.(13)) of the process $e^+e^- \rightarrow \pi^0\gamma$, $\beta_{\pi^0\gamma}$ is a factor taking into account radiative correction (Eq.(14)) and energy spread. Energy (\sqrt{s}) is corrected according to fitted ΔE , its error is 0.08 MeV. The first error of the cross section $\sigma_{\pi^0\gamma}$ is statistical, the second one is systematic.

\sqrt{s} , MeV	δE , MeV	L, nb^{-1}	N	N_{bg}	$\varepsilon_{\pi^0\gamma}$	$\beta_{\pi^0\gamma}$	$\sigma_{\pi^0\gamma}, nb$
599.52	0.14	39.90 ± 0.30	60	46.0	0.315	0.908	$1.23 \pm 0.77 \pm 0.19$
629.51	0.15	46.09 ± 0.33	62	44.8	0.316	0.904	$1.31 \pm 0.68 \pm 0.43$
659.52	0.16	40.02 ± 0.33	37	32.0	0.313	0.899	$0.45 \pm 0.63 \pm 0.17$
689.56	0.19	48.31 ± 0.38	48	33.0	0.316	0.893	$1.10 \pm 0.59 \pm 0.30$
719.51	0.18	58.43 ± 0.43	69	36.0	0.323	0.886	$1.97 \pm 0.56 \pm 0.18$
749.50	0.20	50.90 ± 0.42	84	26.8	0.317	0.866	$4.09 \pm 0.73 \pm 0.28$
759.50	0.20	41.88 ± 0.39	107	20.7	0.316	0.846	$7.71 \pm 1.02 \pm 0.42$
763.50	0.21	38.80 ± 0.38	124	18.7	0.317	0.834	$10.27 \pm 1.19 \pm 0.47$
769.50	0.21	43.60 ± 0.40	234	20.3	0.319	0.812	$18.95 \pm 1.45 \pm 1.08$
773.50	0.21	62.77 ± 0.48	531	28.7	0.319	0.794	$31.62 \pm 1.51 \pm 1.45$
777.50	0.21	76.73 ± 0.53	1544	35.0	0.319	0.776	$79.60 \pm 2.13 \pm 2.15$
778.71	0.22	6.88 ± 0.16	162	3.2	0.319	0.772	$93.89 \pm 8.13 \pm 3.82$
779.48	0.24	43.39 ± 0.39	1282	20.0	0.319	0.770	$118.49 \pm 3.46 \pm 2.94$
780.59	0.23	132.36 ± 0.68	4989	61.4	0.319	0.772	$151.36 \pm 2.20 \pm 4.40$
781.63	0.24	351.62 ± 1.10	15259	164.1	0.319	0.779	$172.82 \pm 1.43 \pm 5.15$
782.52	0.21	81.11 ± 0.53	3523	37.8	0.319	0.793	$169.83 \pm 2.94 \pm 4.76$
783.51	0.21	74.90 ± 0.51	3150	34.7	0.319	0.816	$159.53 \pm 2.93 \pm 5.46$
785.51	0.22	73.73 ± 0.51	2391	33.3	0.320	0.883	$113.15 \pm 2.39 \pm 3.18$
789.50	0.22	56.91 ± 0.46	930	24.6	0.320	1.044	$47.61 \pm 1.66 \pm 1.43$
793.49	0.23	53.03 ± 0.45	456	22.4	0.320	1.201	$21.26 \pm 1.10 \pm 0.80$
799.49	0.23	51.86 ± 0.45	285	21.3	0.320	1.411	$11.27 \pm 0.77 \pm 0.31$
809.49	0.25	65.73 ± 0.52	189	25.8	0.318	1.660	$4.70 \pm 0.43 \pm 0.13$
819.49	0.24	115.74 ± 0.70	233	43.7	0.318	1.775	$2.90 \pm 0.25 \pm 0.19$
839.47	0.25	144.83 ± 0.80	179	52.6	0.320	1.711	$1.59 \pm 0.18 \pm 0.07$
879.45	0.27	170.26 ± 0.91	100	50.4	0.318	1.269	$0.72 \pm 0.16 \pm 0.17$
919.43	0.32	327.70 ± 1.32	137	77.7	0.319	1.048	$0.54 \pm 0.12 \pm 0.04$
939.45	0.30	291.22 ± 1.28	99	63.0	0.318	1.007	$0.39 \pm 0.12 \pm 0.09$
949.45	0.29	259.10 ± 1.22	86	53.9	0.317	0.993	$0.39 \pm 0.13 \pm 0.06$
957.45	0.29	241.63 ± 1.18	79	48.8	0.317	0.984	$0.40 \pm 0.13 \pm 0.06$
969.46	0.30	245.65 ± 1.21	84	47.6	0.319	0.969	$0.48 \pm 0.13 \pm 0.10$

4 Results

Our final results are based on model 2 approximation. Differences in approximation results for models 2–4 were considered as model error contributions to total systematic errors. As a result we present:

$$\sigma_{e^+e^- \rightarrow \omega \rightarrow \pi^0\gamma} = (155.8 \pm 2.7 \pm 4.8) \text{ nb}, \quad (17)$$

$$\sigma_{e^+e^- \rightarrow \rho^0 \rightarrow \pi^0\gamma} = (0.58 \pm 0.13 \pm 0.08) \text{ nb} \quad (18)$$

$$\phi_{\rho\omega} = (-10.2 \pm 6.5 \pm 2.5) \text{ degrees} \quad (19)$$

Detailed point by point listing of the measured $e^+e^- \rightarrow \pi^0\gamma$ cross section is presented in Table 3. Systematic error of the experimental cross section is

determined by systematic errors of integrated luminosity, detection efficiency, radiative correction, and background subtraction. It is worth mentioning that systematic errors for different c.m.s. energy points are highly correlated. Measured cross section and data from [6, 29] are also plotted in Fig.4.

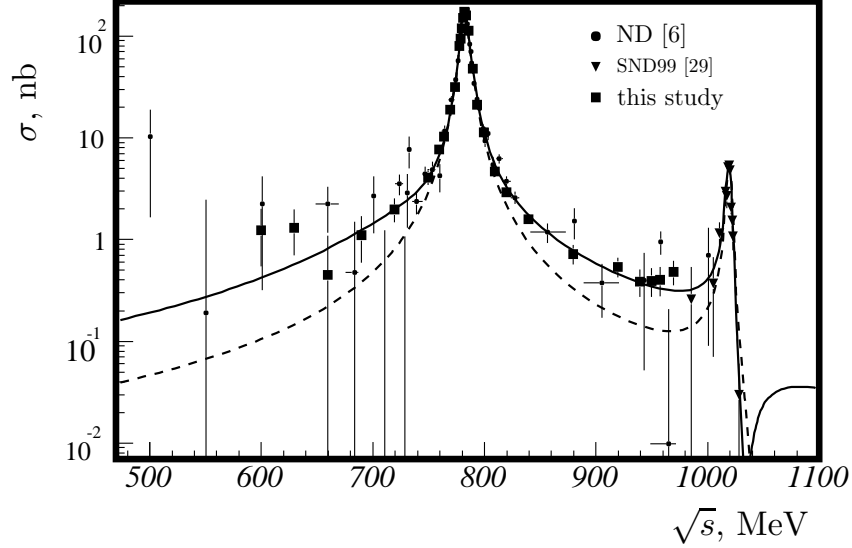


Figure 4: $e^+e^- \rightarrow \pi^0\gamma$ cross section. Solid line depicts the cross section in the model 2, dashed line — in the model 1. Data from ND experiment are grouped by energies and shifted taking into account current world average value of the ω -meson mass.

Decay parameters expressed in terms of probabilities and partial widths are:

$$Br(\omega \rightarrow \pi^0\gamma) \cdot B(\omega \rightarrow e^+e^-) = (6.50 \pm 0.11 \pm 0.20) \times 10^{-6}, \quad (20)$$

$$Br(\rho \rightarrow \pi^0\gamma) \cdot B(\rho \rightarrow e^+e^-) = (2.34 \pm 0.53 \pm 0.33) \times 10^{-8}, \quad (21)$$

$$Br(\omega \rightarrow \pi^0\gamma) = (9.34 \pm 0.15 \pm 0.31) \%, \quad (22)$$

$$Br(\rho^0 \rightarrow \pi^0\gamma) = (5.15 \pm 1.16 \pm 0.73) \times 10^{-4}, \quad (23)$$

$$\Gamma_{\omega \rightarrow \pi^0\gamma} = 788 \pm 12 \pm 27 \text{ keV}, \quad (24)$$

$$\Gamma_{\rho^0 \rightarrow \pi^0\gamma} = 77 \pm 17 \pm 11 \text{ keV} \quad (25)$$

Obtained results statistically agree with previous measurements. The partial width $\Gamma_{\rho^0 \rightarrow \pi^0\gamma}$ is in a good agreement with the world average $\Gamma_{\rho^\pm \rightarrow \pi^\pm\gamma}$. Phenomenological estimates using various models [1, 2, 3, 4, 5] do not contradict our result.

The ratio of the partial widths of the $\omega, \rho \rightarrow \pi^0\gamma$ decays required by strict $SU(3)$ symmetry [2] is equal to 9.47, which agrees with our measurement:

$$\frac{\Gamma_{\omega \rightarrow \pi^0\gamma}}{\Gamma_{\rho^0 \rightarrow \pi^0\gamma}} = 10.3 \pm 2.5 \pm 1.4, \quad (26)$$

5 Conclusions

The most accurate measurement of $e^+e^- \rightarrow \pi^0\gamma$ cross section is performed at the c.m.s. energy region of $0.60 - 0.97$ GeV at the VEPP-2M collider with the SND detector. At present experimental accuracy level this cross section is well described by vector meson dominance model taking into account transitions $\phi, \omega, \rho \rightarrow \pi^0\gamma$. In this model the cross sections of the processes $e^+e^- \rightarrow \omega \rightarrow \pi^0\gamma$ and $e^+e^- \rightarrow \rho^0 \rightarrow \pi^0\gamma$ at corresponding meson masses are measured. Partial widths, their ratios and decay probabilities of corresponding decays were evaluated. Results are presented in Eqs.(17)-(26) and in the Table 3.

Measured values of the $\omega, \rho^0 \rightarrow \pi^0\gamma$ decay parameters are consistent with earlier experimental results. Partial width of the $\rho^0 \rightarrow \pi^0\gamma$ decay is in a good agreement with that of $\rho^\pm \rightarrow \pi^\pm\gamma$ decays. These values also do not contradict various phenomenological estimations. Obtained value of the $\rho - \omega$ interference phase could be well explained by electromagnetic $\rho - \omega$ mixing. Our results have higher accuracy than the world average for $\rho^0 \rightarrow \pi^0\gamma$ and $\omega \rightarrow \pi^0\gamma$.

6 Acknowledgments

This work was partially supported with RFBR grants 00-15-96802, 01-02-16934-a, and grant No.78 1999 of Russian Academy of Science for young scientists.

References

- [1] D.A.Geffen and W. Wilson. *Phys. Rev. Lett.* **44**, 370 (1980).
- [2] P. J. O'Donnell. *Rev. Mod. Phys.* **53**, 673 (1981).
- [3] P.Singer and G.A.Miller. *Phys. Rev.* **D33**, 141–158 (1986).
- [4] N.Barik and P.C.Dash. *Phys. Rev.* **D49**, 299–308 (1994).
- [5] S. lin Zhu et al. *Phys. Lett.* **B420**, 8–12 (1998).
- [6] S.I.Dolinsky et al. *Phys. Rept.* **202**, 99–170 (1991).
- [7] T. Jensen et al. *Phys. Rev.* **D27**, 26 (1983).
- [8] J. Huston et al. *Phys. Rev.* **D33**, 3199 (1986).
- [9] L. Capraro et al. *Nucl. Phys.* **B288**, 659 (1987).
- [10] K. Hagiwara et al. *Phys. Rev.* **D66**, 010001 (2002)
- [11] F.Jacquet et al. *Nuovo Cim.* **63A**, 743 (1969).
- [12] A.B.Baldin et al. *Yad. Fiz.* **13**, 758–764 (1971).
- [13] D.Benaksas et al. *Phys. Lett.* **B42**, 511–514 (1972).

- [14] J.Keyne et al. *Phys. Rev.* **D14**, 28–41 (1976).
- [15] V.M.Aulchenko et al. *J.Exp.Theor.Phys.* **90**, 927–938 (2000),
Zh.Eksp.Teor.Fiz. **90**, 1067–1079 (2000).
- [16] M.N.Achasov et al. *Nucl. Instrum. Meth.* **A449**, 125–139 (2000).
- [17] I.A. Koop et al. *Published in “Physics and detectors for DAPHNE”, Frascati*, 393-404 (1999).
- [18] M.N.Achasov et al. Preprint Budker INP 98-65, Novosibirsk (1998).
- [19] V.V.Anashin et al. Preprint INP 84-123, Novosibirsk (1984).
- [20] A.V.Bozhenok et al. Preprint Budker INP 99-103, Novosibirsk (1999). (in Russian).
- [21] E.A.Kuraev and V.S.Fadin. *Sov. J. Nucl. Phys.* **41**, 466–472 (1985),
Yad. Fiz. **41**, 733–742 (1985).
- [22] G. Bonneau and F. Martin *Nucl. Phys.* **B27**, 381 (1971).
- [23] A.B.Arbutov et al. *JHEP* **10**, 001 (1997).
- [24] E.A.Kuraev and Z.K.Silagadze. *Phys. Atom. Nucl.* **58**, 1741–1743 (1995),
Yad. Fiz. **58**, 1843–1845 (1995).
- [25] V. N. Baier et al. *Phys. Rept.* **78**, 293-393 (1981).
- [26] N.N.Achasov et al. *Sov. J. Nucl. Phys.* **54**, 664–671 (1991),
Yad. Fiz. **54**, 1027–1108 (1991),
Int. J. Mod. Phys. **A7**, 3187–3202 (1992).
- [27] N.N.Achasov et al. *Sov. J. Nucl. Phys.* **55**, 449–459 (1992),
Yad. Fiz. **55**, 809–829 (1992),
Int. J. Mod. Phys. **A7**, 4825–4854 (1992).
- [28] H.B.O’Connell et al. *Prog. Part. Nucl. Phys.* **39**, 201–252 (1997).
- [29] M.N.Achasov et al. *Eur. Phys. J.* **C12**, 25–33 (2000).